μSR-INVESTIGATIONS AT PNPI

S.G. Barsov, S.I. Vorobyev, V.P. Koptev, E.N. Komarov, S.A. Kotov, S.M. Mikirtychyants, G.V. Shcherbakov

1. Investigation of the magnetic properties of homogeneous copper-manganese alloys

In this work, the magnetic properties of homogeneous copper-manganese alloys $Cu_{1-x}Mn_x$ were studied [1] by the muon spin relaxation (μSR) technique at the PNPI synchrocyclotron. Samples were homogenized by quenching in water after their heat treatment in a muffle furnace at a temperature of 1100 K for 100 h.

In our experiments, we measured the time distributions of positrons $N_e(t)$ that were formed as a result of the decay $\mu^+ \to e^+ + \nu_e + \tilde{\nu}_\mu$ (the muon lifetime is $\tau_\mu \approx 2.197 \times 10^{-6}$ s) and emitted in the direction of the initial muon polarization (polarized muon beams were used) in a time window $\Delta t \sim 4.5\tau_\mu$ after each muon was stopped in the sample, as well as the integrated yields of these positrons [2]. The time distributions were approximated by the function

$$N_e(t) = N_0 \cdot [1 + a_0 \cdot G(t)] \cdot \exp(-t/\tau_\mu), \quad (1)$$

where the normalization constant N_0 and the maximum asymmetry a_0 characterize the experimental conditions specific for each sample and do not depend on the muon depolarization. The muon spin relaxation function $G(t)$ determined from the time distribution $N_e(t)$ reflects the effect of local magnetic fields on the muon spin at the site of its stopping. In particular, we have $G(t) = 1$ in the absence of depolarization and $G(t) = 0$ for unpolarized muons.

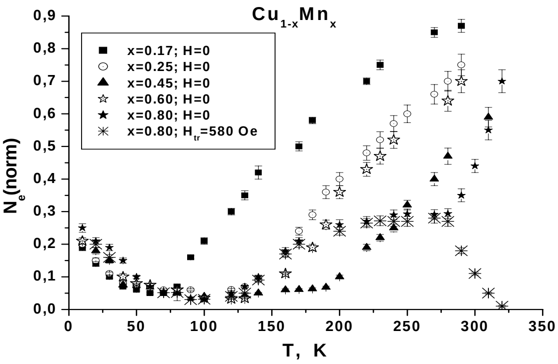

Fig. 1. Temperature dependences of the normalized integrated yield N_e(norm) of positrons for samples with different concentrations of magnetic atoms Mn_x

Figure 1 presents the normalized integrated yields of positrons for samples with different concentrations of magnetic atoms $N_e(\text{norm}) = ((n_e/n_0) - 1)/a_0$. This integrated yield does not depend on the sample geometry, parameters of the muon spin relaxation setup, and muon beam polarization and provides general model-independent information on muon depolarization under local magnetic fields. The parameters n_0 and a_0 were determined at a temperature considerably higher than the temperature of the transition to the magnetically ordered phase.

Specifically, the normalized integrated yield N_e(norm) measured for the $Cu_{0.2}Mn_{0.8}$ sample at temperatures $T > 330$ K in zero magnetic field tends to unity. This circumstance suggests the absence of muon depolarization in the far paramagnetic range in which the frequency of oscillations of electronic moments is too high ($\sim 10^{12}$ Hz) for their magnetic field to change substantially the muon polarization. The paramagnetic state is also indicated by the complete depolarization of muons in a relatively weak transverse external magnetic field of ~580 Oe. In the temperature range 290−320 K, the normalized integrated yield N_e(norm) changes drastically and then reaches a value of ~1/3. This suggests that the sample transforms into a magnetically ordered state with an isotropic (on a local, cluster or domain level) orientation of static internal local magnetic field. This behavior is in good agreement with the phase diagram previously proposed by A. Banerjee and A.K. Majumdar [Phys. Rev. B **46**, 8958 (1992)], according to which the antiferromagnetic transition at $T_N \sim 300$ K occurs in a homogeneous alloy with the concentration $x = 0.8$. The normalized integrated yield N_e(norm) equal to 1/3 is retained to $T \approx 200$ K. With a further decrease in the temperature, the normalized integrated yield N_e(norm) decreases sharply almost to zero. This indicates that in the given temperature range a strong dynamic depolarization of muons arises. The temperature dependence of the normalized integrated yield N_e(norm) in the range 20–200 K is characteristic of frustrated magnets which undergo transition to a low-temperature spin-glass state through an intermediate magnetically ordered phase with a long-range order. In this case, the dynamic polarization is associated with the transformation of the magnetic structure in the transition range [3].

The temperature dependence of the normalized integrated yield N_e(norm) for the samples with the concentration $x = 0.17$, 0.25, and 0.45 are also plotted in Fig. 1. The normalized integrated yield N_e(norm) for these samples decreases drastically with a decrease in the temperature due to the strong depolarization of muons. Since the normalized integrated yield N_e(norm) decreases almost to zero, the inference can be made that the arising local magnetic fields have a fluctuation character and are rather high. Moreover, the normalized integrated yield N_e(norm) for the sample with the concentration of manganese atoms $x = 0.45$ initially decreases to a small value and then remains virtually unchanged over a wide temperature range (from 60 to 200 K). This suggests to some extent that, in the given temperature range, the sample is in a specific phase state characterized by a fast spin dynamics. As the temperature decreases ($T < 60$ K), the normalized integrated yield N_e(norm) increases gradually to the value of ~1/3 which corresponds to the transition of the sample to the isotopic magnetic phase with a slow spin dynamics.

It should be noted that the dependence of the normalized integrated yield N_e(norm) on the concentration x of magnetic manganese atoms exhibits one more feature. The rate of change in the normalized integrated yield N_e(norm) with a variation in the temperature in the high-temperature transition range is identical for all samples with concentrations $x = 0.17$–0.60. This indicates once again that the same physical processes occur in the alloys and that the characteristics obtained are not associated with the specific quality of the samples. The transition temperature increases with an increase in the concentration of magnetic atoms to $x = 0.45$. A further increase in the concentration of magnetic atoms is accompanied by a decrease in the transition temperature. For example, the transition temperature for the sample with the concentration $x = 0.60$ is approximately equal to that for the sample with the concentration $x = 0.25$. A similar dependence of the transition temperature on the concentration x was observed by Banerjee and Majumdar. This effect was explained by the corresponding change in the size of antiferromagnetic clusters.

The analysis of the time spectra $N_e(t)$ demonstrates that the experimental data cannot be described using simple relaxation functions. In the paramagnetic range, the experimental data are well described by the relaxation function

$$G\,(t) = \exp\,(-\lambda \cdot t). \qquad (2)$$

However, as the temperature of the first magnetic transition is approached (this can be judged from the drastic increase in the relaxation rate λ), the description of the experimental data requires the use of the relaxation function in the form of the sum of two exponential functions; that is

$$G(t) = a_1 \cdot \exp(-\lambda_D \cdot t) + a_2 \cdot \exp(-\lambda \cdot t), \qquad (3)$$

where $a_1 + a_2 = 1$, $G(t)$ is the dimensionless relaxation function varying from 0 to 1, and λ_D and λ are the dynamic relaxation rates for the corresponding exponential function. The experimental data are best described using constant parameters $a_1 = 1/3$ and $a_2 = 2/3$.

At temperatures below 100 K, the experimental data for the samples can be described by the following relaxation function:

$$G(t) = [1/3 + 2/3 \cdot (1 - \Delta \cdot t) \cdot \exp(-\Delta \cdot t)] \cdot \exp(-\lambda_D \cdot t). \qquad (4)$$

For $\lambda_D << \Delta$ this form of the relaxation function G is consistent with the spin-glass model. In this case, the parameter λ_D corresponds to the relaxation associated with the occurrence of fluctuating random fields. The parameter Δ is connected to the static fields.

A more complex expression for the relaxation function was proposed by Uemura *et al*. [Phys. Rev. B **31**, 546 (1985)]. However, when describing the time spectra $N_e(t)$ for samples with high manganese concentrations ($x > 0.2$) the form of the relaxation function represented by expression (4) is more preferential.

The behavior of the relaxation functions for the $Cu_{0.55}Mn_{0.45}$ sample with a variation in the temperature is illustrated in Figs. 2, 3. It can be seen from these Figures that a virtually complete depolarization of the muon ensemble is observed in the temperature range 120–240 K. The relaxation function decreases only when the temperature of the sample decreases below a temperature of 100 K. At a temperature of 20 K, the relaxation function asymptotically approaches a value of ~1/3 which corresponds to the isotropic orientation of quasi-static local magnetic fields.

The temperature dependences of the parameters λ, λ_D, and Δ are shown in Fig. 4. There are two magnetic phase transitions. The first transition in the sample is observed at a temperature of ~200 K, and the second transition occurs at temperatures in the range 130–150 K.

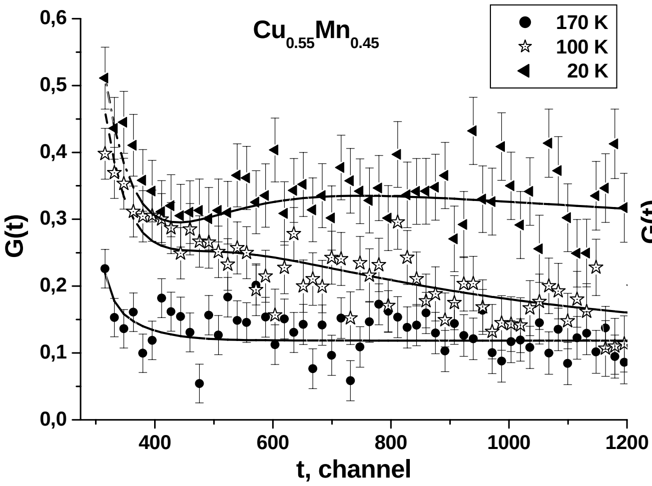

Fig. 2. Relaxation functions for the $Cu_{0.55}Mn_{0.45}$ sample at different temperatures in the range 170–300 K. One channel on the time scale corresponds to 0.625 ns. The origin of the scale is located at the 274^{th} channel

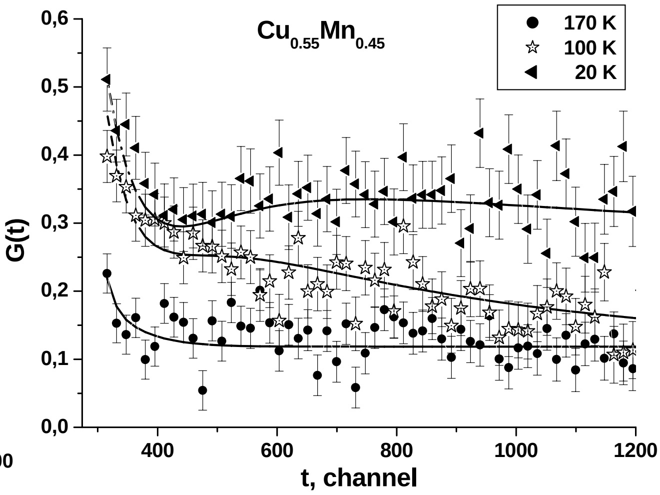

Fig. 3. Relaxation functions for the $Cu_{0.55}Mn_{0.45}$ sample at different temperatures in the range 20–170 K. One channel on the time scale corresponds to 0.625 ns. The origin of the scale is located at the 274^{th} channel

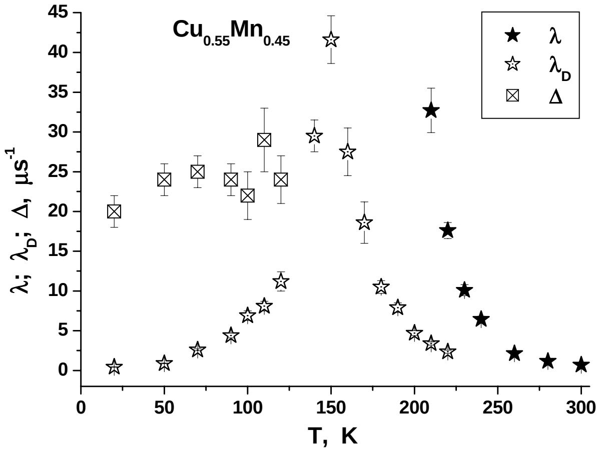

Fig. 4. Temperature dependences of the dynamic (λ, λ_D) and static (Δ) relaxation rates

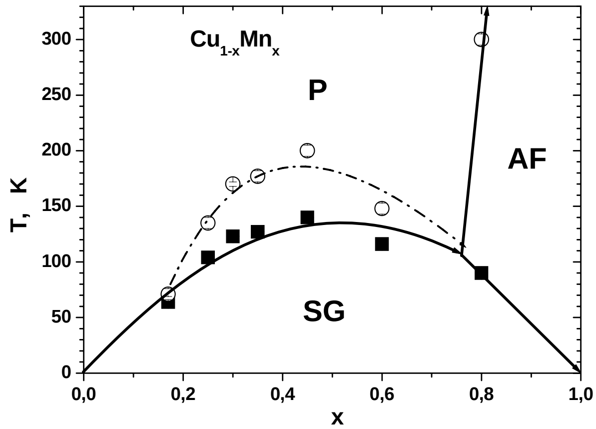

Fig. 5. Phase diagram of the homogeneous copper-manganese alloys $Cu_{1-x}Mn_x$

It should be noted that the static-field parameter Δ can be obtained by processing the experimental data only in the case where $\Delta > \lambda_D$. Note also that a decrease in the parameter λ_D leads to an increase in the reliability for determining the static-field parameter Δ.

Therefore, the results obtained demonstrate that in the homogeneous alloys $Cu_{1-x}Mn_x$ over a wide range of concentrations, there exists a phase transition to a specific magnetic state at temperatures in the range 100–200 K. This phase arises irrespective of the type of the high-temperature state, *i.e.* the paramagnetic or antiferromagnetic state. The new phase is characterized by a considerable non-uniformity of local fields due to the absence of a long-range magnetic order.

Thus, the data obtained make it possible to complement substantially the magnetic phase diagram of the homogeneous copper-manganese alloys $Cu_{1-x}Mn_x$ (Fig. 5). This phase diagram takes the form characteristic of systems with competing exchange interactions [3].

In the phase diagram depicted in Fig. 5 the solid line indicates the boundaries between the paramagnetic (P), antiferromagnetic (AF), and spin-glass (SG) states according to the data available in the literature. Points (○) and (■) correspond to the results obtained in the present work for the high- and low- temperature transitions, respectively. The dot-dashed line represents the conventional boundary of the existence of the new phase state between the paramagnetic and spin-glass phases. As can be seen in Fig. 5, the concentration dependence $T(x)$ does not contradict the tendency of the change in the temperature T_G of the transition to the spin-glass state for concentrations $x < 0.15$. The largest temperature range between two transitions is observed at concentrations $x \sim 0.5$. The experimental results indicate that the new phase is characterized by a fast spin dynamics not only in the vicinity of the transition but also at lower temperatures down to the temperature of the transition to the spin-glass state. The analysis of the experimental data obtained allows us to assume that two magnetically ordered phases can be formed in the $Cu_{1-x}Mn_x$ binary alloys at relatively high concentrations of magnetic manganese atoms in the temperature range from 20 to 250 K. At temperatures below ~180 K there arises a state with a fast spin dynamics and fluctuating random fields. In this state, the parameters λ_D and Δ are of the same order of magnitude. The experimental data obtained can be described using complex relaxation functions $G(t)$ [expressions (3), (4)]. At a temperature of ~100 K the transition to the spin-glass phase without fluctuating random fields, *i.e.* the conventional spin-glass phase, is observed in the alloys for all the concentrations under investigation.

2. The study of the magnetic properties of the $(Pd_{1-x}Fe_x)_{0.95}Mn_{0.05}$ alloy

The measurements were performed both in a zero external magnetic field and in various transverse magnetic fields over the temperature range 10–300 K [4, 5]. The behavior of the relaxation parameter λ allows determination of the phase transition point, since a sharp increase in λ is observed near this point due to critical fluctuations. Figure 6 shows the temperature dependence of the dynamic relaxation rate $\lambda(T)$; we can see a pronounced peak in λ at $T_C = 39.5$ K which suggests that critical fluctuations develop near this temperature.

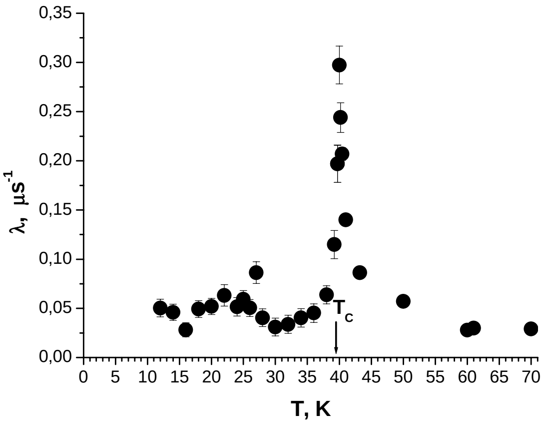

Fig. 6. Temperature dependence of the dynamic relaxation rates λ

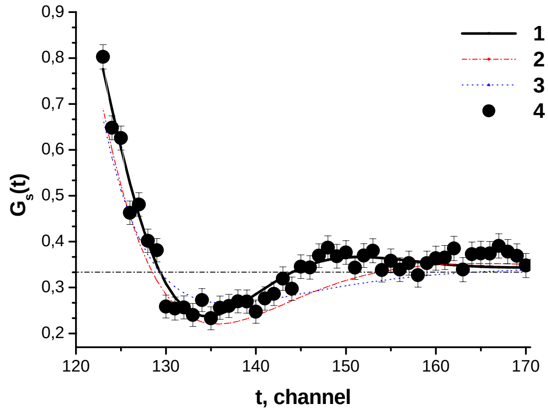

Fig. 7. Muon spin relaxation function: (1) processing within the CFM model with χ^2=1.02, (2) processing within the ASM model with χ^2=2.26, (3) processing within the SG model with χ^2=2.6, and (4) experimental points obtained at T = 28 K in a field H_{ext} = 0. One channel on the time axis corresponds to 5 ns

A further analysis of the experimental data showed that, below $T_C = 39.5$ K, the description of $G(t)$ will have the best value of χ^2 in the collinear-ferromagnet (CFM) model (Fig. 7)

$$G(t) = [1/3 + 2/3\,(\cos(\Omega\cdot t)\cdot\exp(-\Delta\cdot t))]\cdot\exp(-\lambda\cdot t). \quad (5)$$

The distribution function of local static fields is a Lorentzian with the average magnetic field H and the magnetic field variance Δ (Fig. 8); the temperature dependence at $T > 25$ K can be described by the relation $H \sim H_{max}(1 - T/T_C)^{\beta}$, where the value $\beta \approx 0.40 \pm 0.02$ corresponds to the model of the Heisenberg-type 3D magnet.

As the temperature decreases further (below 25 K), the χ^2-parametr changes and the confidence level decreases down to zero. The experimental data in Fig. 8 significantly deviate from the fitting curve and are poorly described by the model based on relation (5). None of the hypotheses proposed in Ref. [2] (CFM, asperomagnet (ASM), and spin glass (SG)) yields a more or less adequate description of the G function. The value $\chi^2 = 1$ at 97% confidence level was achieved only in the case when the experimental data are processed using the sum of two functions, CFM+SG (Fig. 9),

$$G(t)=(a_{CFM}\cdot(1/3 + 2/3\cdot\cos(H_0\cdot t)\cdot\exp(-\Delta_{CFM}\cdot t))+a_{SG}\cdot(1/3 + 2/3\cdot(1-\Delta_{SG}\cdot t)\cdot\exp(-\Delta_{SG}\cdot t)))\cdot\exp(-\lambda\cdot t), \qquad (6)$$

where $a_{CFM} + a_{SG} = a_S$ is the initial decay asymmetry.

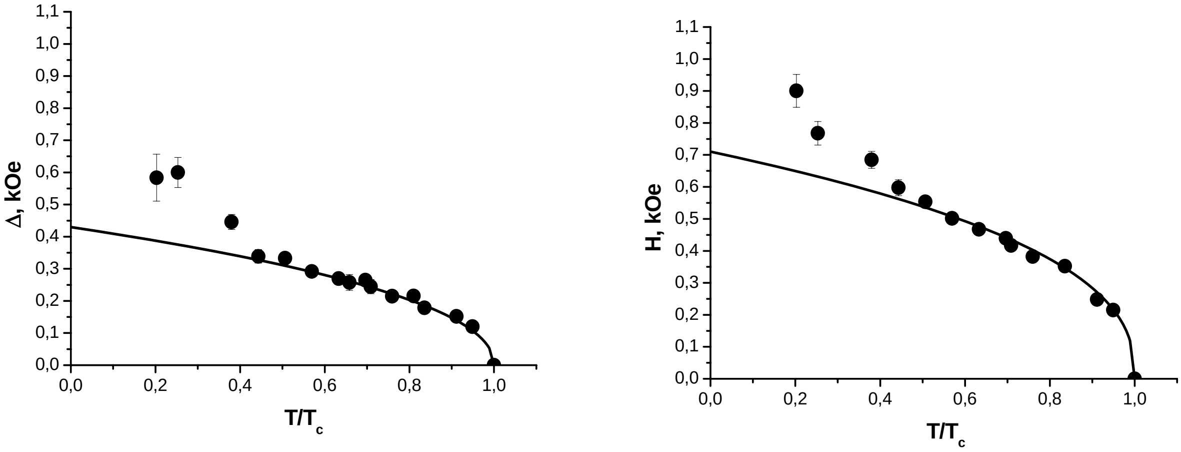

Fig. 8. Temperature dependence of the variance Δ of static fields and the average field H. The curves are fitting of the experimental data using the relation $H \sim H_{max}(1 - T/T_C)^{\beta}$, where $\beta \approx 0.40 \pm 0.02$ corresponds to the model of the Heisenberg-type 3D magnet

By writing the initial decay asymmetry in the form of a sum of two terms describing different states, we can separate both contributions. Thus, we can conclude that two phase states coexist simultaneously in the sample below 25 K; one of these states is ferromagnetic and the other is the spin-glass state. This conclusion is consistent with the model presented by relation (6). Figure 10 shows the temperature dependence of the ratio of the spin-glass fraction asymmetry to the maximum asymmetry. It can be seen that, as the temperature decreases, the spin-glass fraction increases long before the transition to the spin-glass state.

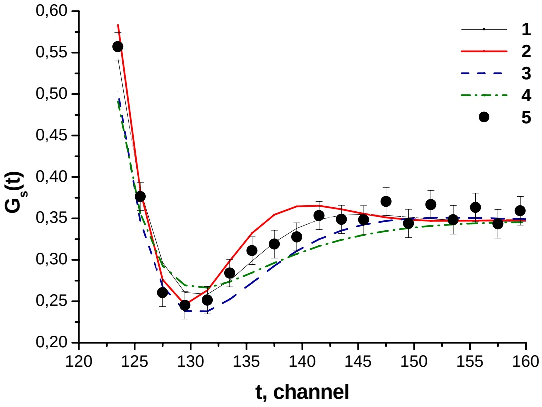

Fig. 9. Muon spin relaxation function: (1) the description by the sum of two functions CFM+SG with χ^2=1.0, (2) processing within the CFM model with χ^2=1.23, (3) processing within the ASM model with χ^2=1.58, (4) processing within the SG model with χ^2=1.85, and (5) experimental points obtained at T=15 K in a zero external field. One channel on the time axis t corresponds to 5 ns

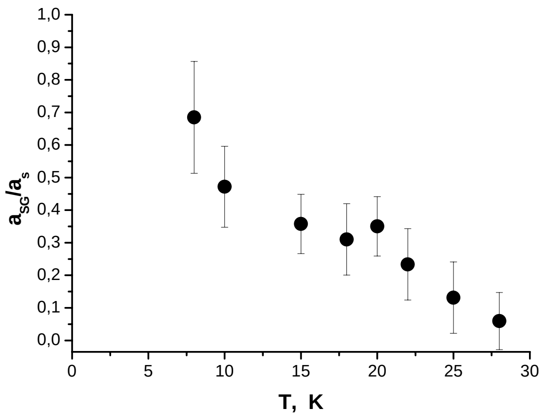

Fig. 10. Temperature dependence of the fraction of the spin-glass contribution to the depolarization of a muon ensemble

An analysis of the distributions of local magnetic fields shows that various magnetic states occur in the $(Pd_{0.984}Fe_{0.016})_{0.95}Mn_{0.05}$ alloy as temperature is varied (Fig. 8). For example, in the temperature range $25 < T < 39$ K this alloy is in the CFM state with a Lorentzian distribution of local magnetic fields. In the temperature range $10 < T < 25$ K, the magnetic structure of the alloy can be considered as a superposition of a collinear ferromagnet

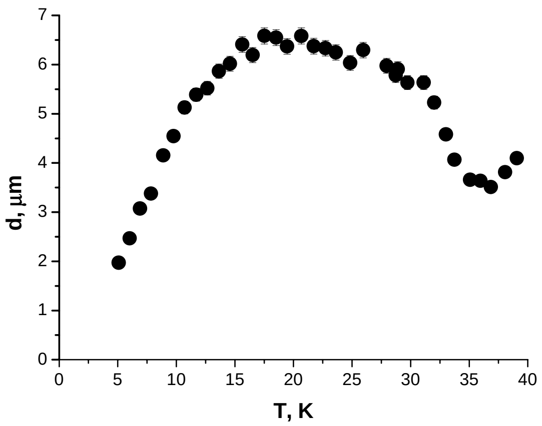

Fig. 11. Temperature dependence of the average size of magnetic inhomogeneities under cooling in a zero field

and a spin glass with a Lorentzian distribution of local magnetic fields. Below T = 10 K, the alloy probably undergoes a transition to the SG phase.

We also calculated the size d of magnetic inhomogeneities. To estimate it, we used the data on neutron depolarization ΔP obtained upon sample cooling under the ZFC conditions. We note that the temperature dependence of the depolarization ΔP under these conditions is characteristic of samples without magnetic anisotropy (the so-called 3/2 rule is valid). The quantity d (the average size of a domain or a cluster) is calculated with allowance for the sample magnetic isotropy and assuming that the average magnetization M_{inh} of inhomogeneities is equal to the average field H (Fig. 8). The results of this calculation are shown in Fig. 11.

3. Muon investigation of $HoMnO_3$ and $YMnO_3$ hexagonal manganites

Manganites $RMnO_3$ exhibit a wide variety of physical properties, depending on the rare-earth element R. Compounds with a large ion radius of the element R (La, Pr, Nd, Sm, Eu, Gd, and Tb) are crystallized in the orthorhombic structure with the space group *Pnma*. Compounds with a smaller ion radius of the element R (Ho, Er, Tm, Yb, Lu, Y, Sc, and In) exhibit the hexagonal crystal structure with the space group $P6_3cm$. The hexagonal manganites belong to ferroelectromagnetic materials in which the transition temperature to the ferroelectric state, $T_C \sim 600-1000$ K, is much higher than the temperature of antiferromagnetic ordering, $T_N \sim 70-130$ K.

This work is devoted to the investigation of local magnetic fields and their distribution in multiferroics $HoMnO_3$ and $YMnO_3$ by the μSR-method of substance investigation [6]. The samples were obtained by the solid-phase synthesis method. The measurements were performed on the muon channel of the PNPI synchrocyclotron using a μSR setup [7].

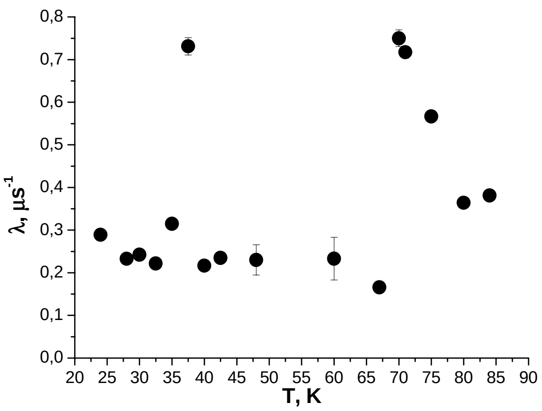

Fig. 12. Relaxation rate of the polarization of muons stopped in the $HoMnO_3$ sample in zero magnetic field

Figure 12 shows the temperature dependence of the relaxation rate λ, of the polarization of muons stopped in the $HoMnO_3$ sample in zero magnetic field. This dependence exhibits two peaks at 76 K and 40 K, which correspond to two phase transitions. The first transition at T = 76 K is a transition from the paramagnetic state to the antiferromagnetic ordering state. The second transition at T = 40 K is associated with the rotation of the spins of Mn by 90° (spin-relaxation transition). This conclusion is in good agreement with results obtained by other methods [B. Lorenz *et al.*, Phys. Rev. Lett. **92**, 087204 (2004)].

Detailed analysis of the muon polarization relaxation function G makes it possible to determine the parameters of the distribution of local magnetic fields at various temperatures of the samples under investigation. In particular, the relaxation function of the polarization of muons stopped in the $HoMnO_3$ sample, $G(t)$, in zero magnetic field is described by the expression

$$G(t) = [a_1\cdot(1/3+2/3\cdot\cos(\Omega_1\cdot t)\cdot\exp(-\Delta_1\cdot t)) + a_2\cdot(1/3 + 2/3\cdot\cos(\Omega_2\cdot t)\cdot\exp(-\Delta_2\cdot t))]\cdot\exp(-\lambda\cdot t), \quad (7)$$

where $a_1 + a_2 = a_S$ is the initial asymmetry of the decay of muons stopped in the sample, λ is the dynamical relaxation rate, $\Omega_{1,2} = 2\pi\cdot F_{1,2}$ are the cyclic frequencies (associated with the mean local field at the muon localization site), and $\Delta_{1,2}$ are the frequency spreads associated with the spread of internal magnetic fields.

Figure 13 shows the temperature dependence of the frequencies of the muon spin precession for the $HoMnO_3$ sample in zero external magnetic field. It is seen that precession at two frequencies, one of which is negligibly low as compared to the other frequency ($F_1 \approx 40$ MHz and $F_2 < 1$ MHz), is observed for sample

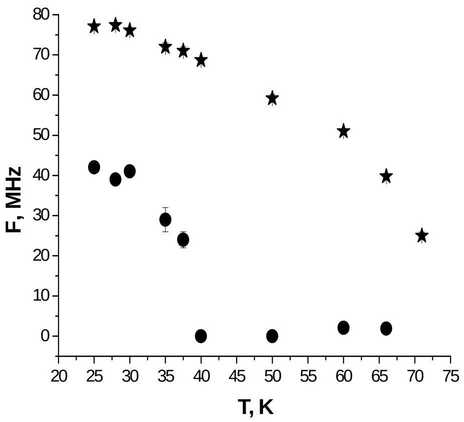

Fig. 13. Temperature dependence of frequencies (stars) F_1 and (circles) F_2 of the precession observed for the $HoMnO_3$ sample in zero field

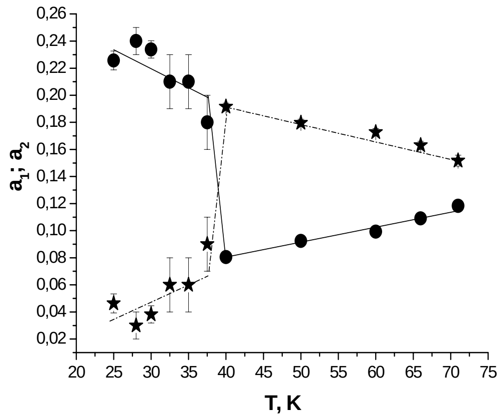

Fig. 14. Temperature dependence of the asymmetry coefficient (stars) a_1 and (circles) a_2, where $a_1 + a_2 = a_S$, for the $HoMnO_3$ sample in zero field. The lines are drawn to guide the eye

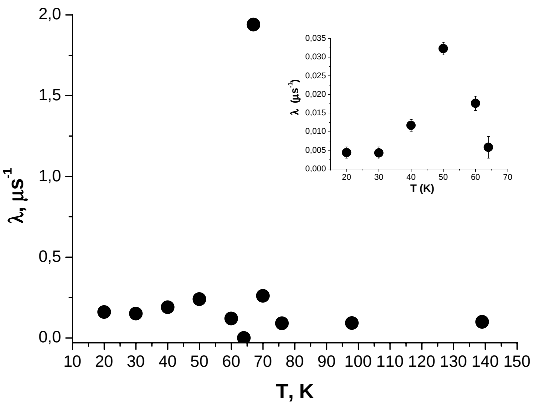

Fig. 15. Temperature dependence of the polarization relaxation rate for muons stopped in the $YMnO_3$ sample in zero field

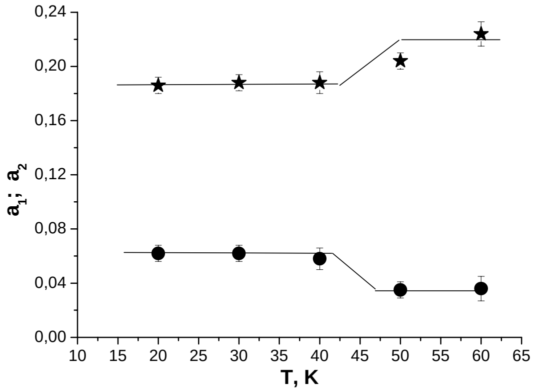

Fig. 16. Temperature dependence of the asymmetry coefficient (stars) a_1 and (circles) a_2, where $a_1 + a_2 = a_S$, for the $YMnO_3$ sample in zero field. The lines are drawn to guide the eye

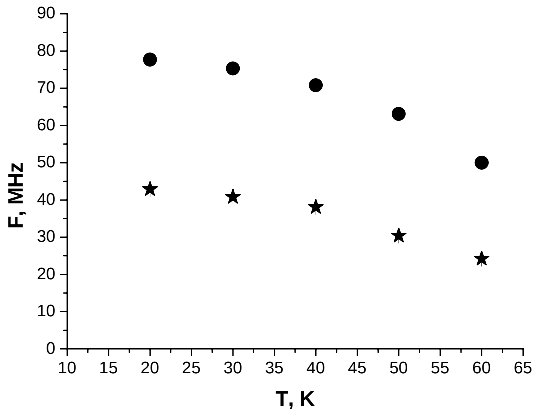

Fig. 17. Temperature dependence of the frequencies (stars) F_1 and (circles) F_2 of the precession observed for the $YMnO_3$ sample in zero field

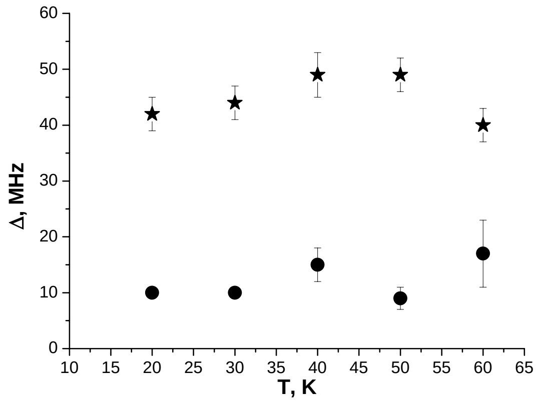

Fig. 18. Temperature dependence of the parameters (stars) Δ_1 and (circles) Δ_2 for the $YMnO_3$ sample

temperatures below $T = 76$ K. As the sample temperature is decreased, F_1 increases monotonically, whereas F_2 decreases. For sample temperatures below the temperature $T_{SR} = 42$ K, the frequency F_2 increases noticeably (almost from zero) and continues to increase monotonically with decreasing the temperature.

Figure 14 shows the temperature dependence of the coefficients a_1 and a_2 (see Eq. (7)). It is seen that the relation between the coefficients a_1 and a_2 changes sharply at the temperature of the spin-rotation transition, $T_{SR} = 42$ K.

Similar investigations were performed for the $YMnO_3$ sample. Figures 15−18 show the results of the processing of the experimental data obtained with the $YMnO_3$ samples. The temperature dependence of the polarization relaxation rate λ for muons stopped in the $YMnO_3$ sample exhibits a peak at a temperature of $T = 66$ K, which corresponds to the paramagnetic-antiferromagnetic phase transition (see Fig. 15). A non-monotonic temperature behavior of the parameter λ is seen in the temperature interval of 45−55 K (see the inset in Fig. 15). The precession at two frequencies F_1 and F_2 is seen in the temperature interval of 20−60 K; the relation between the frequencies, $F_2/F_1 \approx 2$, holds in the indicated temperature interval (Fig. 17).

Figure 18 shows the temperature dependence of the parameters Δ_1 and Δ_2 (frequency spread) in the temperature interval of 20−60 K. Similar results were obtained by T. Lancaster *et al*. [Phys. Rev. Lett. **98**, 197203 (2007)].

Note a feature in the behavior of the partial amplitudes a_1 and a_2 in the temperature interval of 20−60 K. A change in the ratio of these parameters, a_1/a_2, is observed at a temperature of $T \approx 50$ K (see Fig. 16). Thus, the temperature dependences of the relaxation rate of the muon spin (shown in Fig. 15) and partial amplitudes a_1 and a_2 (shown in Fig. 16) for the $YMnO_3$ sample exhibit features at a temperature of ~50 K. This is likely attributed to the partial rotation of the manganese spins in the $YMnO_3$ compound obtained by P.J. Brown and T. Chatterji [J. Phys.: Condens. Matter **18**, 10085 (2006)].

The temperature dependence of the precession frequency for the $HoMnO_3$ and $YMnO_3$ samples is well approximated by the Curie-Weiss curve, $F \sim F_{max}(1 - T/T_N)^{\beta}$ with the value $\beta = 0.39 \pm 0.02$ corresponding to the Heisenberg 3D magnet model.

4. Influence of magnetic nanoparticles on behavior of polarized positive muons in ferrofluid on the Fe_3O_4 base in carrier medium D_2O

The ferrofluid on the basis of the Fe_3O_4 nanoparticles dispersed in heavy water (D_2O) have been investigated by means of the μSR-method. It was revealed that the distinct muonium precession signal is observed simultaneously with the muon (diamagnetic) precession signal. The behaviour of the muon and muonium fractions in the ferrofluid is compared with those in the pure heavy water. The experiment was carried out at temperatures 50−300 K in transverse magnetic fields of 7.76 Oe and 278 Oe. It was observed that the muon (diamagnetic) fraction is created in the ferrofluid approximately in the same proportion as in D_2O, however the muon spin relaxation rate to a considerable extent is higher in the ferrofluid than in D_2O at temperatures $T > 150$ K. A part of the muonium fraction at these temperatures essentially less in the ferrofluid than in D_2O. The precession frequencies of the muon and muonium spins in a ferrofluid is noticeably lower than in D_2O.

References

1. S.G. Barsov, S.I. Vorobyev, V.P. Koptev *et al.*, Physics of Solid State **49**, 1740 (2007).
2. S.G. Barsov, A.L. Getalov, V.P. Koptev *et al.*, Preprint PNPI-1312, Gatchina, 1988. 17 p.
3. S.G. Barsov, A.L. Getalov, S.L. Ginsburg *et al.*, Hyperfine Interactions **64**, 415 (1990).
4. S.G. Barsov, S.I. Vorobyev, V.P. Koptev *et al.*, Preprint PNPI-2688, Gatchina, 2006. 17 p.
5. S.G. Barsov, S.I. Vorobyev, V.P. Koptev *et al.*, Physics of Solid State **49**, 1492 (2007).
6. S.G. Barsov, S.I. Vorobyev, V.P. Koptev *et al.*, JETP Lett. **85**, 658 (2007).
7. S.G. Barsov, S.I. Vorobyev, V.P. Koptev *et al.*, Preprint PNPI-2694, Gatchina, 2006. 17 p.